ALICE Internal Note
2002-034

LHC Experimental Conditions [1]

A. Morsch and I. Pshenichnov

Editors: A. Morsch, F. Carminati, Y. Foka, P. Giubellino, G. Paic, J.-P. Revol, K. Šafařík, U.A. Wiedemann

Abstract

ALICE is the dedicated heavy-ion experiment at the LHC. This note describes the experimental conditions at the LHC, such as luminosities, collision systems and the radiation environment.

[1] This note is Chapter 2 of the ALICE Physics Performance Report (PPR). Thus it contains some cross references to other chapters of the PPR.

Contents

2 LHC experimental conditions

Chapter 1 has summarized the observables relevant to the physics goals of ALICE. Whether ALICE can reach these goals does not only depend on the performance of the detectors, but also on the number of events which can be collected, the number of collision systems which can be studied and last but not least on the background conditions at the LHC. The number of collected events depends on the nature of the beam, the luminosity and the running time. Therefore, we first describe in this chapter our proposed running strategy, followed by a discussion of the required luminosity for each collision systems including luminosity limitations of both the detector and the LHC machine complex. Then we describe the expected background conditions at the LHC. In the last section of this chapter the ALICE luminosity monitoring and determination is outlined.

2.1 Running Strategy

Like the SPS and RHIC programs, a comprehensive heavy ion program at the LHC will be based on two components: colliding the largest available nuclei at the highest possible energy and a limited systematic study of different collision systems (pp, pA, AA) and of different beam energies. As the number of possible combinations of collision systems and energies is very large, careful and constant updating of priorities is required in order to optimise the physics output. We have therefore divided the ALICE program into two phases: An initial program with priorities based on our current theoretical understanding and the results from SPS and RHIC, and a later stage with a number of options whose relative importance is likely to become clear only after the first data has been analysed at LHC.

The LHC is expected to run essentially in the same yearly mode as the SPS, starting with several months of pp running followed at the end of each year by several weeks of heavy ion collisions. For rate estimates, all LHC experiments use an effective time per year of $10^7 s$ for pp and $10^6 s$ for heavy ion operation.

ALICE will take its first data with pp collisions, because the LHC will be commissioned with proton beams, but also because pp physics is an integral part of the ALICE program. ALICE will in fact require some minimum amount of pp running throughout its operation: During the initial few years longer periods to both commission the detector and to take pp physics data, and later in the program shorter periods to start-up and calibrate the detector prior to every heavy ion period.

Pb–Pb collisions, which provide the highest energy density, are foreseen immediately after the end of the first pp run. Even if of short duration and at low initial luminosity, this first physics pilot run will provide already a wealth of information on global event properties and large cross section observables, as it was the case during the very successful commissioning of RHIC. For low cross section observables, in particular the hard processes which are a main focus at the LHC, some further $1-2$ years of Pb–Pb runs at the highest possible luminosity should provide sufficient statistics. One period of pPb running is required early on, most likely in the 3^{rd} year of LHC operation. This will provide reference data and will allow to determine nuclear modifications of the nucleon structure functions (shadowing), which is necessary for the interpretation of the Pb–Pb data. The best way to study energy density dependencies is to use lower-mass ion systems, which can been selected from a list of candidates suitable for the CERN ion source. We plan to study first Ar–Ar collisions over a period of $1-2$ years. This initial ALICE program, which has been discussed and endorsed by the LHCC, is summarised below:

- Regular pp runs at $\sqrt{s} = 14\,\mathrm{TeV}$
- Initial heavy ion program
  - Pb–Pb physics pilot run

- 1 – 2 years Pb–Pb
- 1 year pPb like collisions (pPb, dPb or αPb)
- 1 – 2 years Ar–Ar

For the later phase, we have considered a number of running options, the relative importance of which will depend on the initial results. For a direct comparison of the Pb–Pb and pp data, a dedicated pp run at the Pb–Pb centre of

mass energy, $\sqrt{s_{\rm NN}} = 5.5\,\text{TeV}$, is probably advisable. A more complete energy density scan would require additional intermediate-mass ion runs. To map out the the *A*-dependence further pA runs with different nuclei could be necessary. Additional Pb–Pb runs at lower energy would allow to measure an energy excitation function and to connect to the RHIC results. Finally, some rare processes limited by statistics in the early runs could require additional high-energy Pb–Pb running. The list of running options for the second phase is summarised below:

- Later options, some of them depending on the outcome of the initial data analysis
  - Dedicated pp or pp-like (dd or αα) collisions at $\sqrt{s_{\rm NN}} = 5.5\,\text{TeV}$
  - Possibly another intermediate mass A–A system (N–N, O–O, Kr–Kr or Sn–Sn)
  - Possibly another pA (dA, αA) system
  - Possibly lower energy Pb–Pb runs
  - Further high energy Pb–Pb runs

2.2 Pb–Pb collisions

2.2.1 Pb–Pb luminosity limits from detectors

The luminosity for Pb–Pb collisions is an important issue, because there are limitations coming from both the detector and the accelerator. We start with the limitations due to the ALICE detector. The limits are coming from the main tracking device, the Time Projection Chamber (TPC) and the Forward Muon Spectrometer, which are considered separately.

The TPC limits the maximum usable luminosity because of event pile-up during the 90 μs drift time. At a luminosity of $10^{27}\,\text{cm}^{-2}\text{s}^{-1}$, the pile-up probability is 76 % for a hadronic interaction cross-section of 8 barn. However, since the average particle multiplicity amounts to only 20% of the maximum multiplicity and since only partial events overlap, the average increase of the track multiplicity due to pile up is about 13% for central collisions. Locally the track density increases by up to 26%. It is conceivable that the TPC can be operated at luminosities above $10^{27}\,\text{cm}^{-2}\text{s}^{-1}$, in particular, if the multiplicity turns out to be low. However, the gain in rate has to be weighted against the loss in tracking performance. The luminosity limitation of the muon spectrometer comes from the maximum acceptable illumination of the trigger chambers, Resistive Plate Chambers (RPC) of $50 - 100\,\text{Hz}\,\text{cm}^{-2}$. This limit corresponds to a maximum usable luminosity of $(2-4)\times 10^{28}\,\text{cm}^{-2}\text{s}^{-1}$. As will be shown in the following section, the limitations from the machine are stronger than those coming from the ALICE detector, which justify the choice of detector technologies.

2.2.2 Nominal luminosity Pb–Pb runs

For a given initial luminosity (L_0), optimal operation requires a maximization of the time averaged luminosity $\langle L \rangle$ given by

$$\langle L \rangle(t) = \frac{1}{t+T_{\rm f}} \int_{t_{\rm set-up}}^{t} {\rm d}t' L\,(t'). \tag{2.1}$$

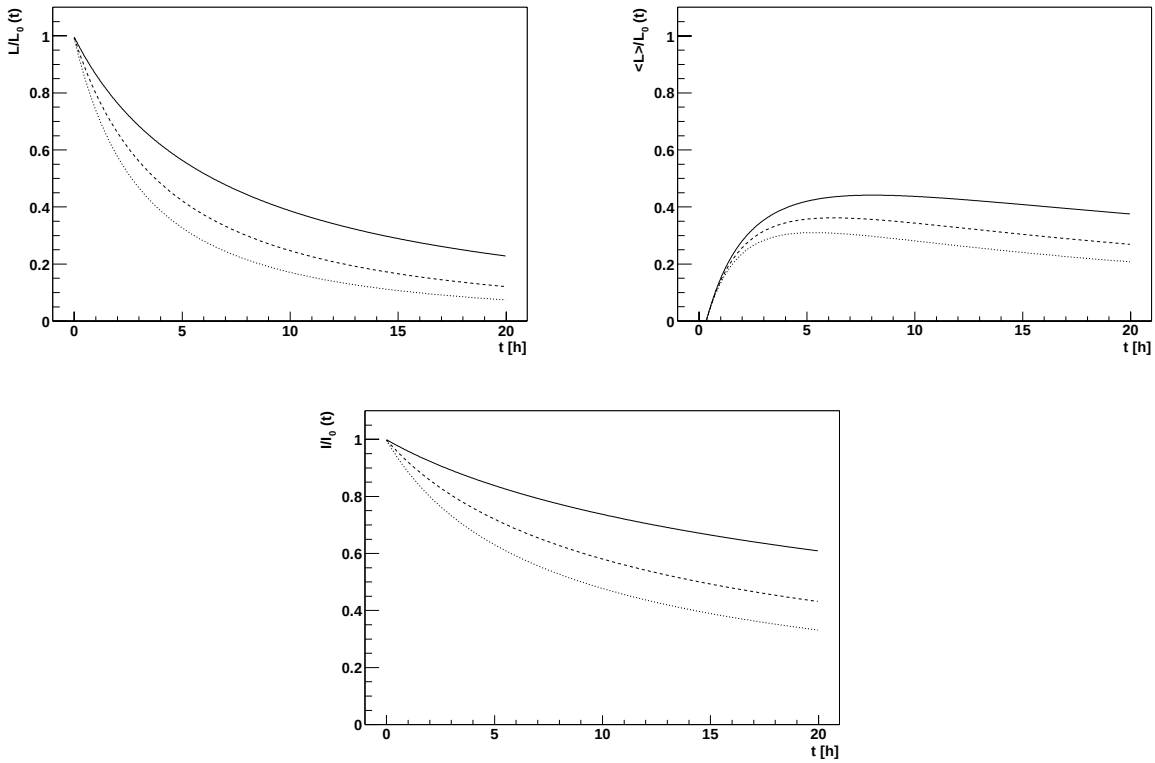

Figure 2.1: Luminosity, average luminosity relative to $L_0 = 10^{27}\,\mathrm{cm}^{-2}\mathrm{s}^{-1}$ and beam intensity relative to $I_0 = 6.8 \times 10^7$ ions per bunch for nominal operation with Pb–Pb collisions in one (solid line), two (dashed line) and three (dotted line) interaction regions.

Here T_f is the filling time and $t_{\mathrm{set-up}}$ the experiment set-up time, i.e. the time during which the collider is operating but the experiment is not yet taking data. The high electromagnetic cross-section for removing Pb ions from the beam, $\simeq 500\,\mathrm{barn}$, is the main limit for the luminosity lifetime. The lifetime depends on how many experiments are active during the ion runs. Using $\beta^* = 0.5\,\mathrm{m}$ which requires the smallest beam intensity, the half-life for an initial luminosity $L_0 = 10^{27}\,\mathrm{cm}^{-2}\mathrm{s}^{-1}$ are 6.7 h for one, 3.1 h for two, and 2.7 h for three experiments (see Ref. [1] using updated cross-sections from [2]).

Figure 2.1 shows the luminosity and time-averaged luminosity relative to $L_0 = 10^{27}\,\mathrm{cm}^{-2}\mathrm{s}^{-1}$ for nominal operation with Pb–Pb collisions in one, two and three interaction regions. A filling time of 3 h and experiment set-up time of 20 min are assumed. The average luminosity has a plateau at around 8 h. At this time the average luminosities are $0.44L_0$, $0.35L_0$ and $0.29L_0$ for one, two and three experiments, respectively. Although the luminosity evolution is shown for up to 20 h of running time, in reality, the sensitivity of the beam position monitors, minimum 3×10^9 charges per bunch, limits the running time to 15 h for two experiments and 9 h for three experiments participating in the run.

2.2.3 Alternative Pb–Pb running scenarios

For a fixed L_0 the luminosity lifetime is proportional to the beam intensity. Hence, longer lifetimes can be obtained in high-β^* high-intensity runs. The luminosity optimization is constrained by three effects: intra-beam scattering, longitudinal emittance growth, and the maximum beam intensity. Intra-beam scattering plays a role because the emittance growth time is inversely proportional to the beam intensity. The relative longitudinal emittance growth must be less than a factor of two to avoid beam losses. Finally, the beam intensity is constrained by space charge limits in the SPS.

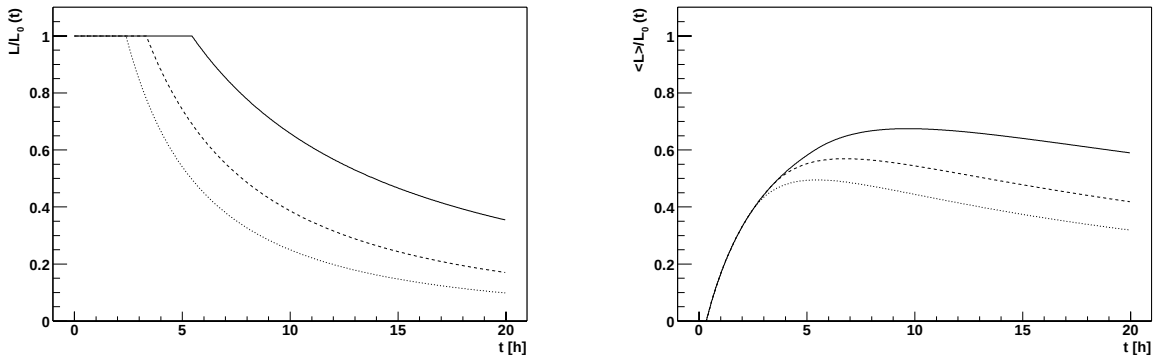

Figure 2.2: Luminosity and average luminosity relative to L_0 for β^*-tuning operation with Pb–Pb collisions in one (solid line), two (dashed line) and three (dotted line) interaction regions. This scenario assumes an intensity of 10^8 Pb ions per bunch, the highest envisaged intensity.

At the nominal initial luminosity, running at $\beta^* = 2\,\mathrm{m}$ and consequently twice the nominal beam intensity, the average luminosity increases by only $\simeq 10\%$. A further, and much more important, increase of the average luminosity is possible by β^*-tuning, decreasing β^* during the run to keep the luminosity constant until the minimum β^*, 0.5 m, is reached. The maximum possible bunch intensity corresponds to about 1.4 times the nominal intensity. Using β^*-tuning with this intensity could increase the average luminosity by approximately a factor of 1.6 as shown in Fig. 2.2.

β^*-tuning is also very important for operation with the nominal initial beam intensity. It can be shown that using β^*-tuning the same average luminosity as anticipated for an initial luminosity of $L_0 = 10^{27}\,\mathrm{cm^{-2}s^{-1}}$ can be reached with a lower initial luminosity: $0.7L_0$, $0.55L_0$ and $0.5L_0$ for one, two and three experiments, respectively [3]. This has two important advantages. First, a constant luminosity during the run makes it easier to handle space charge effect in the TPC. Secondly, operation at a lower initial luminosity is safer for the machine, because the quench limit mentioned above might be close to the nominal L_0.

Since the ALICE measurement of Υ production in the forward muon spectrometer is statistics limited, ALICE would profit from dedicated high luminosity Pb–Pb runs. The same scheme as described above, high intensity and tuned β^*, can be applied. It is currently assumed that the maximum Pb–Pb luminosity is limited to $(0.5-1)\times 10^{27}\,\mathrm{cm^{-2}s^{-1}}$ by the maximum allowed beam-pipe heating in the cold machine elements of the dispersion suppressor, the quench limit. The energy deposition in these elements comes from Pb ions lost in electromagnetic interactions [1, 4].

2.2.4 Beam energy

Short runs of a few days each at lower beam energies may be requested to study the energy as well as Bjorken-*x* dependence of global hadronic event features. These runs at the lowest possible beam energy will help to bridge the gap in energy between the top RHIC energy of $\sqrt{s_{\mathrm{NN}}} = 200\,\mathrm{GeV}$ and the LHC. More complete energy excitation functions in observables such as multiplicity, transverse-momentum spectra, particle ratios, will then be obtained.

2.3 Intermediate-mass ion collisions

To vary the energy density, ALICE will study at least one intermediate-mass system during the first 5 years. The currently envisaged choice is Ar–Ar. Fig.2.3 shows the approximate energy-density bands covered by varying the impact parameter for several systems. Using medium central collisions in several

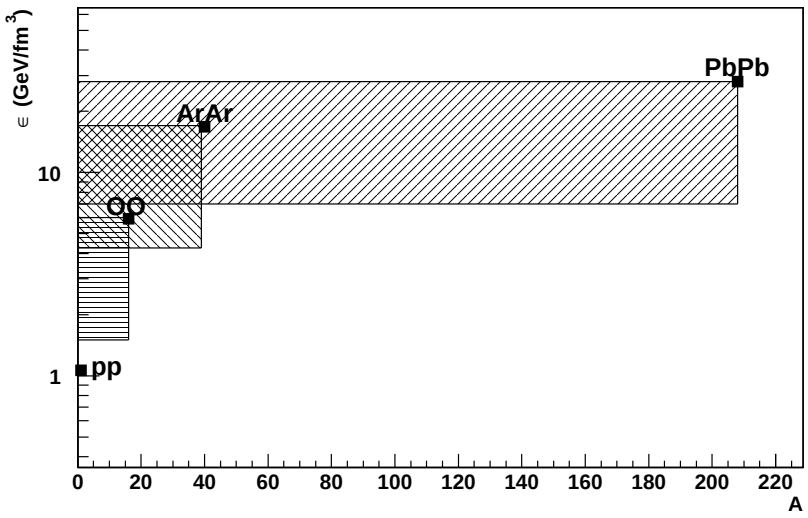

Figure 2.3: Variation of the produced energy density with collision system. The energy density has been calculated using the Bjorken formula $\varepsilon = 160\text{MeV fm}^{-3} A^{-2/3} \mathrm{d}N_{\mathrm{ch}}/\mathrm{d}y$, with maximum charged particle multiplicities of 6000, 1200, 230 and 6.5 for central Pb–Pb, Ar–Ar, O–O, and pp collisions, respectively. The bands show the approximate range covered by changing the impact parameter. In pp collisions the energy density can be increased by up to a factor 10 selecting high multiplicity events.

Table 2.1: Maximum bunch intensities allowed by space-charge effects in the SPS and the corresponding maximum and average luminosities for one (two, three) experiments participating in the run. The limits for Ar–Ar and O–O are preliminary estimates.

System	Ions per bunch	$L_0(\text{cm}^{-2}\text{s}^{-1})$	$\langle L \rangle / L_0$
Pb–Pb	7.0×10^7	1.0×10^{27}	0.44 (0.35, 0.29)
Ar–Ar	5.5×10^8	0.6×10^{29}	0.56 (0.50, 0.44)
O–O	1.0×10^9	2.0×10^{29}	0.73 (0.70, 0.67)

systems to vary the energy density has the advantage of keeping the collision geometry similar, thus simplifying the interpretation of the data. Other options suitable for LHC (Sn–Sn, Kr–Kr, N–N, O–O) will possibly be required in later runs. The final choice will depend on the physics outcome.

Two maximum luminosities will be considered for Ar–Ar interactions: $L = 2.8 \times 10^{27}\,\text{cm}^{-2}\text{s}^{-1}$ to match the Pb–Pb rates and $L = 10^{29}\,\text{cm}^{-2}\text{s}^{-1}$ to maximize the heavy vector-meson rate in the dimuon decay channel. The corresponding luminosities for low and high luminosity O–O runs are $5.5 \times 10^{27}\,\text{cm}^{-2}\text{s}^{-1}$ and $2 \times 10^{29}\,\text{cm}^{-2}\text{s}^{-1}$, respectively.

The same limitations from space charge effects in the SPS for Pb–Pb also apply to intermediate-mass ions. Presently, only the limits for Pb–Pb collisions have been studied in detail. Scaling from the Pb–Pb values results in the scenario presented in Table 2.1. Only 60% of the required high Ar–Ar luminosity can be delivered by the machine while the required high O–O luminosity is at the limit.

2.4 Proton–proton collisions

2.4.1 Standard pp collisions at $\sqrt{s} = 14\,\mathrm{TeV}$

Since pp collisions are needed to obtain reference data and are of intrinsic interest, they are an integral part of the heavy-ion physics program [5, 6]. Moreover, pp runs will provide low multiplicity, thus simpler, data to commission and calibrate the components of the ALICE detector. Hence, they are needed during the whole ALICE operation.

In order to keep the pile-up in the TPC and Silicon Drift Detectors (SDD) at an acceptable level, the luminosity during pp runs has to be limited to $\simeq 3\times10^{30}\,\mathrm{cm^{-2}s^{-1}}$, corresponding to an interaction rate of $\simeq 200\,\mathrm{kHz}$. At this rate, we record on average 20 overlapping events. Then 95% of the data volume correspond to unused partial events unless an efficient high-level trigger is used for data compression. Optimal operation with the TPC, i.e. no pile-up, is at $\simeq 10^{29}\,\mathrm{cm^{-2}s^{-1}}$. Hence, ALICE will request a luminosity range from $10^{29}\,\mathrm{cm^{-2}s^{-1}}$ to $10^{31}\,\mathrm{cm^{-2}s^{-1}}$ at IP2.

For the muon spectrometer the highest acceptable luminosity of about $5\times10^{31}\,\mathrm{cm^{-2}s^{-1}}$ is set by the RPC illumination limit.

The pp runs will be in parallel with the other experiments but at reduced luminosities. Depending on the beam intensity and emittance the luminosity reduction can be obtained either by running with a higher β^*, $50-200\,\mathrm{m}$ for a reduction by factor $100-400$, or with displaced beams. This will be discussed in more detail in Section 2.6.

2.4.2 Dedicated pp-like collisions (low-energy pp, dd or $\alpha\alpha$)

Optionally, pp-like collisions close to the heavy-ion center-of-mass energy, $\sqrt{s_{\mathrm{NN}}} = 5.5-7\,\mathrm{TeV}$, might be needed for further reference data, such as resolving ambiguities in Monte Carlo extrapolations from $\sqrt{s} = 14\,\mathrm{TeV}$ to the A–A center-of-mass energies.

Collisions of very low-mass ions, such as d or α, can be treated in most cases as systems of independent nucleons. The center-of-mass energy per nucleon pair is 7 TeV in the LHC nominal configuration. These collisions have the additional advantage of having factors of 4 (dd) and 16 ($\alpha\alpha$) higher hard cross-sections as compared to pp collisions compensating for the shorter runs.

Limiting the interaction rate to 200 kHz, as in standard pp, the required luminosities are $1.1\times10^{30}\,\mathrm{cm^{-2}s^{-1}}$ and $6.2\times10^{29}\,\mathrm{cm^{-2}s^{-1}}$ for dd and $\alpha\alpha$, respectively. The net gain, taking into account the lower luminosities, in the hard interaction rate is a factor of 1.5 in dd and a factor of 3.3 in $\alpha\alpha$.

2.5 pA collisions

In addition to pp reference data, pA collisions are also needed for reference data and for studying gluon shadowing. They are thus an integral part of the heavy-ion physics program.

The optimal luminosity in pA runs is rate and not lifetime limited [3]. Constraints exist from the source and the injection. However, since the luminosity is proportional to the product of the two beam intensities and since high-intensity proton beams are available, the ion-beam intensity can be optimized accordingly. Limiting the collision rate to 200 kHz, as in pp collisions, leads to luminosities of $1.1\times10^{29}\,\mathrm{cm^{-2}s^{-1}}$ and $3\times10^{29}\,\mathrm{cm^{-2}s^{-1}}$ for pPb and pAr collisions, respectively.

For asymmetric collision systems like pA, Z/A ratio is very different for the two beams leading to different nominal momenta, 7 TeV for protons and about 3.5 TeV for ions. One consequence is, that the center-of-mass energy per nucleon pair given by

$$\sqrt{s_{\mathrm{NN}}} = 14\,\mathrm{TeV}\times\sqrt{\frac{Z_1Z_2}{A_1A_2}} \tag{2.2}$$

is higher in pA collisions ($14\,\mathrm{TeV}\times\sqrt{Z/A}$) compared to A–A ones ($14\,\mathrm{TeV}\times Z/A$).

Table 2.2: Maximum energies, rapidity shifts, geometric cross-sections, and lower and upper limits on luminosities for several different symmetric and asymmetric systems.

System	$\sqrt{s_{\mathrm{NN}}}_{\mathrm{max}}$ (TeV)	Δy	σ_{geom}(barn)	$L_{\mathrm{low}}(\mathrm{cm}^{-2}\mathrm{s}^{-1})$	$L_{\mathrm{high}}(\mathrm{cm}^{-2}\mathrm{s}^{-1})$
Pb–Pb	5.5	0	7.7	1.0×10^{27}	
Ar–Ar	6.3	0	2.7	2.8×10^{27}	1.0×10^{29}
O–O	7.0	0	1.4	5.5×10^{27}	2.0×10^{29}
αα	7.0	0	0.34	6.2×10^{29}	
dd	7.0	0	0.19	1.1×10^{30}	
pp	14.0	0	0.07	3.0×10^{30}	
pPb	8.8	0.47	1.9	1.1×10^{29}	
pAr	9.4	0.40	0.72	3.0×10^{29}	
pO	9.9	0.35	0.39	5.4×10^{29}	
dPb	6.2	0.12	2.6	8.1×10^{28}	
dAr	6.6	0.05	1.1	1.9×10^{29}	
dO	7.0	0.00	0.66	3.2×10^{29}	
αPb	6.2	0.12	2.75	7.7×10^{28}	
αAr	6.6	0.05	1.22	1.7×10^{29}	
αO	7.0	0.00	0.76	2.8×10^{29}	

Another consequence is that the center-of-mass system of the collision moves with respect to the laboratory system. This movement corresponds to a shift of the central rapidity Δy observed in the laboratory system

$$\Delta y = 0.5 \ln \frac{Z_1 A_2}{Z_2 A_1}. \tag{2.3}$$

Alternatively, dA or αA collisions may have the advantage that they are more symmetric in Z/A. Hence, the center-of-mass energy per nucleon pair is closer to those of heavy-ion collisions: 6.2 TeV (6.6 TeV) for dPb (dAr) collisions as compared to 8.8 TeV (9.4 TeV) for pPb (pAr) ones. Furthermore, the central rapidity is less shifted: 0.12 (0) for dPb (dAr) collisions as compared to 0.46 (0.40) for pPb (pAr) ones.

The luminosity limits are summarized in Table 2.2.

Table 2.3: LHC machine parameters for pp and Pb–Pb runs for ALICE.

	pp	Pb–Pb
Energy per nucleon (TeV)	7	2.76
β at the IP (collisions) (m)	10	0.5
r.m.s. beam radius at IP (μm)	71	16
r.m.s. bunch length (cm)	7.5	7.5
r.m.s. vertex spread (cm)	5.3	5.0
Vertical crossing half-angle (μrad)	100	75
Number of bunches	2808	592
Bunch spacing (ns)	25 [a]	100
Number of particles per bunch	1.1×10^{11}	6.8×10^{7}
Luminosity ($\mathrm{cm}^{-2}\mathrm{s}^{-1}$)	$< 3 \times 10^{30}$	10^{27}

[a] If the electron cloud effect limits the minimum bunch spacing during early operation, a bunch spacing of 50 ns will be used.

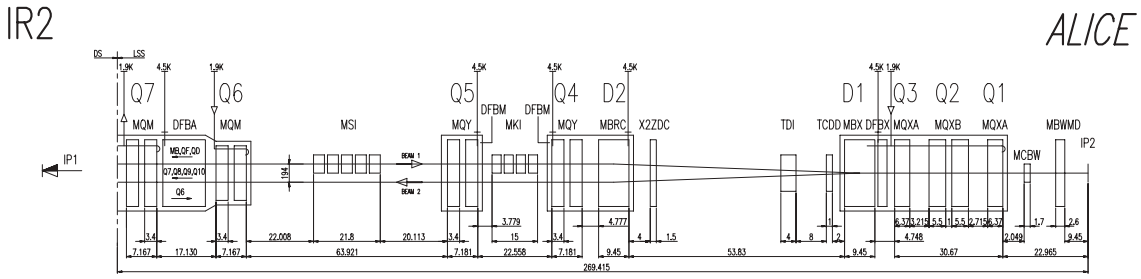

Figure 2.4: Location of beam elements for the IR2 region.

2.6 Machine parameters

In Table 2.3, the LHC machine parameters for pp and Pb–Pb operation are summarized.

Luminosity reduction in pp runs

In the present nominal design, the IR2 optics will work in the pp-collision mode for a $\beta^* = 10\,\mathrm{m}$ as shown in Figs. 2.4 and 2.5. Thus the luminosity is reduced by only a factor of 20 compared to the dedicated high-luminosity experiments, not enough to reach the desired luminosity of about $3 \times 10^{30}\,\mathrm{cm}^{-2}\mathrm{s}^{-1}$. An additional reduction can be obtained by displacing the two beam centers at the interaction point by a distance d. The reduction factor f_R obtained in this way is

$$f_\mathrm{R} = \exp\left(-\frac{d^2}{4\sigma^2}\right), \tag{2.4}$$

where σ is the transverse beam size. We need $d/\sigma = 4.5$ to reduce the luminosity to $3 \times 10^{30}\,\mathrm{cm}^{-2}\mathrm{s}^{-1}$ at full bunch intensity.

During the LHC running-in phase, beam intensities and luminosities are lower than their nominal values. Although the present design values, Table 2.4, do not allow for such a scenario, it could well be that during some limited time the beam intensities are so low that defocussing is enough to reach

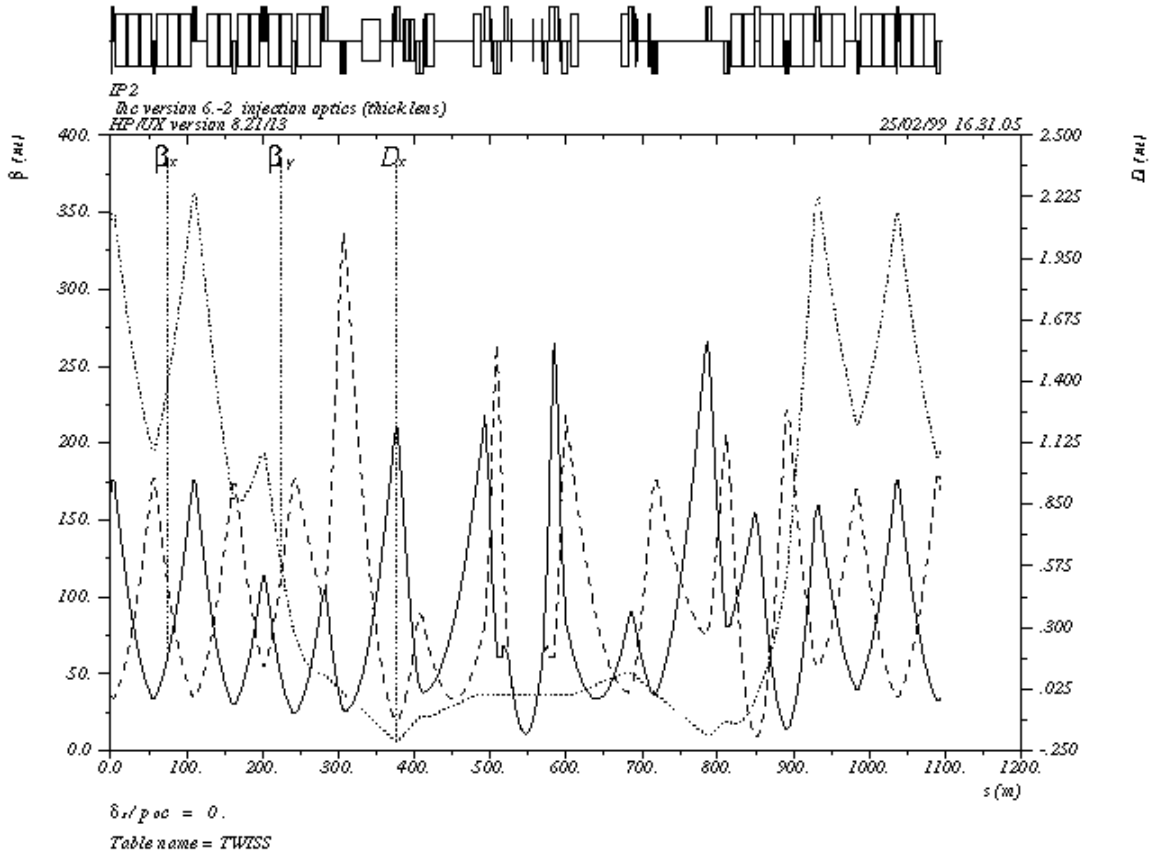

Figure 2.5: Optical functions for Ring 1 close to IR2 for $\beta^* = 10\,\mathrm{m}$.

Table 2.4: LHC pp operation parameters. If the electron-cloud effect limits the minimum bunch spacing during early operation, a bunch spacing of 50 ns will be used.

Scenario	Number of bunches	Protons per bunch	Bunch spacing (ns)	Normalized emittance (nm)	L ($\mathrm{cm^{-2}s^{-1}}$)
nominal	2808	1.10×10^{11}	25	3.75	1.0×10^{34}
early operation	2520	2.75×10^{10}	25	1.00	2.1×10^{33}

the desired luminosity. Since we expect to obtain the most stable running conditions without beam displacement we asked the SL division to calculate the maximum β^* for a range of beam intensities. At present $\beta^* \simeq 100\,\mathrm{m}$ does not seem impossible and would yield a factor of 200 reduction.

2.7 Radiation environment

2.7.1 Background conditions in pp

2.7.1.1 Background from beam–gas collisions in the experimental region

The dynamic gas pressure inside the experimental region, $\pm 20\,\mathrm{m}$ around the interaction point, has been simulated [9]. The considered dynamic effects comprise proton beam-induced phenomena: ion, electron and photon stimulated molecular desorption, ion-induced desorption instability and electron cloud build-up. It has been shown that electron-cloud build-up is the dominant effect. The simulations assume a stainless-steel beam pipe with TiZrV sputtered NEG over the whole surface and ion pumps at about $\pm 20\,\mathrm{cm}$ from the interaction point. The resulting hydrogen-equivalent gas density in proton operation amounts to $\simeq 2 \times 10^{14}\,\mathrm{molecules/m^3}$. For Pb operation the gas density is expected to be two orders of magnitude lower. The gas density in proton operation leads at full current to a beam–gas interaction rate of $12\,\mathrm{kHz/m}$, i.e. $500\,\mathrm{kHz}$ integrated over the ALICE experimental region region, to be compared to the pp collision rate of 200 kHz.

2.7.1.2 Background from the IR2 straight section

The dynamic gas densities in the Dispersion Suppressor (DS) and the Long Straight Section (LSS) of the insertion region IR2, excluding the experimental beam pipe, $\pm 20\,\mathrm{m}$, have been estimated for beam optics version 6.3 and for the first years of running [10]. The dynamic gas density at LHC is determined by ion, photon and electron stimulated desorption. The latter two change with absorbed dose, so that results have been presented for a specific run scenario during the first years of LHC operation. The results have been obtained using very pessimistic assumptions, i.e. no NEG pumping in the elements at room temperature and a factor of 100 overestimate of the out-gassing rate inside the TDI. After discussing the issue with the vacuum group, it has been agreed that the realistic reference for background simulation should be the third year scenario presented in Ref. [10] with the gas pressure inside the TDI scaled down by a factor of 100, shown in Fig. 2.6.

Based on these realistic gas pressure calculations, the fluxes of secondary particles induced by the proton losses upstream and downstream of IR2 was estimated [11]. The new and more realistic gas pressures lead to fluxes of muons and hadrons at the entrance of the experimental regions higher than previously estimated, by up to a factor of 10.

An output file has been provided to the ALICE collaboration containing the particles types and momentum vectors of particles entering the experimental region. The particle statistical weight has been normalized to one proton–gas interaction per second and per meter. Knowing the distance to the

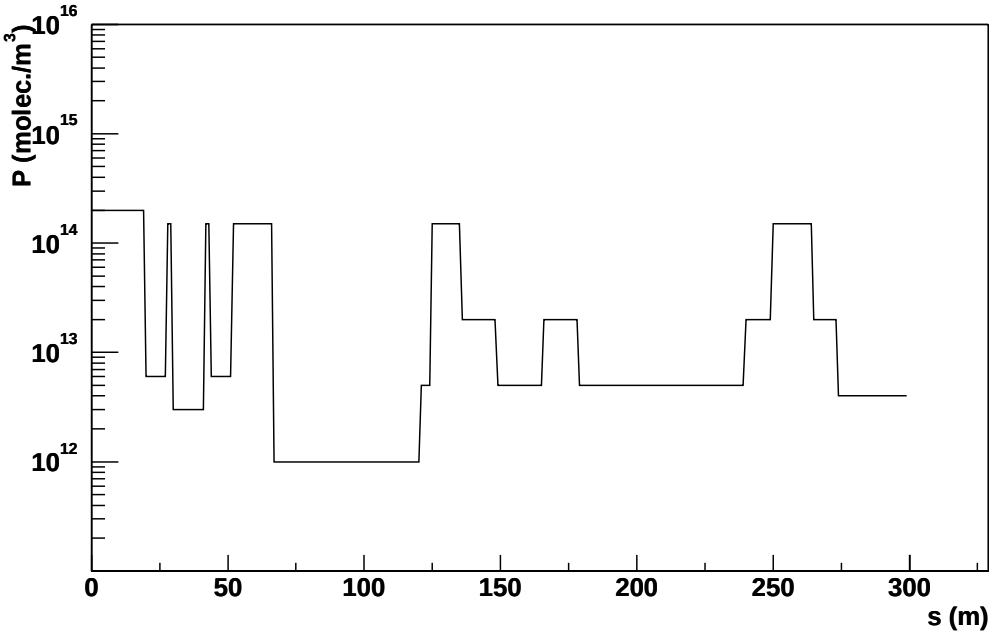

Figure 2.6: Gas-pressure distribution for IR2 in the first three years of LHC operation estimated after some days of operation as a function of the distance from interaction point.

interaction point for primary proton–gas collisions, we are able to perform background simulations for the ALICE experiment for different gas-pressure distributions. The muon and hadron fluxes at the tunnel entrance as a function of the distance to the beam pipe are shown in Fig. 2.7. The maximum muon flux is $\simeq 3.5\,\mathrm{Hz/cm^2}$ whereas the hadron flux has a wide plateau of $\simeq 30\,\mathrm{Hz/cm^2}$ and a maximum of $1\,\mathrm{MHz/cm^2}$ inside the beam pipe. Hadrons outside the beam pipe, $r = 3\,\mathrm{cm}$, will be shielded. By far more dangerous are the particles that enter the experimental area inside the beam pipe since they will shower further downstream closer to the ALICE central detectors.

2.7.2 Dose rates and neutron fluences

We will take data with proton and light- or heavy-ion beams for different time periods and different luminosities. The radiation load on the various parts of the detectors must therefore be calculated for a combination of beam conditions. There are three major sources of radiation in ALICE:

- particles produced at the interaction point in planned collisions;
- beam losses due to mis-injection since ALICE is located near the injection point;
- beam–gas interactions in pp operation.

It has been shown that beam–gas interactions and beam losses contribute, respectively, 10% and 1% to the total dose and neutron fluence [12]. The dominant contribution comes from particles produced at the interaction point.

In Table 2.5 we present a typical scenario for ten years of operation. It includes ten years of pp operation and five years each of Pb–Pb and Ar–Ar (or dPb) runs. The Ar–Ar runs are split into low- and high-luminosity runs. The table shows the average luminosity, the number of expected minimum-bias collisions and the total charged-particle multiplicity per event as well as the total number of produced charges. The latter number suggests the relative contributions to the total dose. In this scenario, 80% of the radiation dose is from pp and Ar–Ar operation.

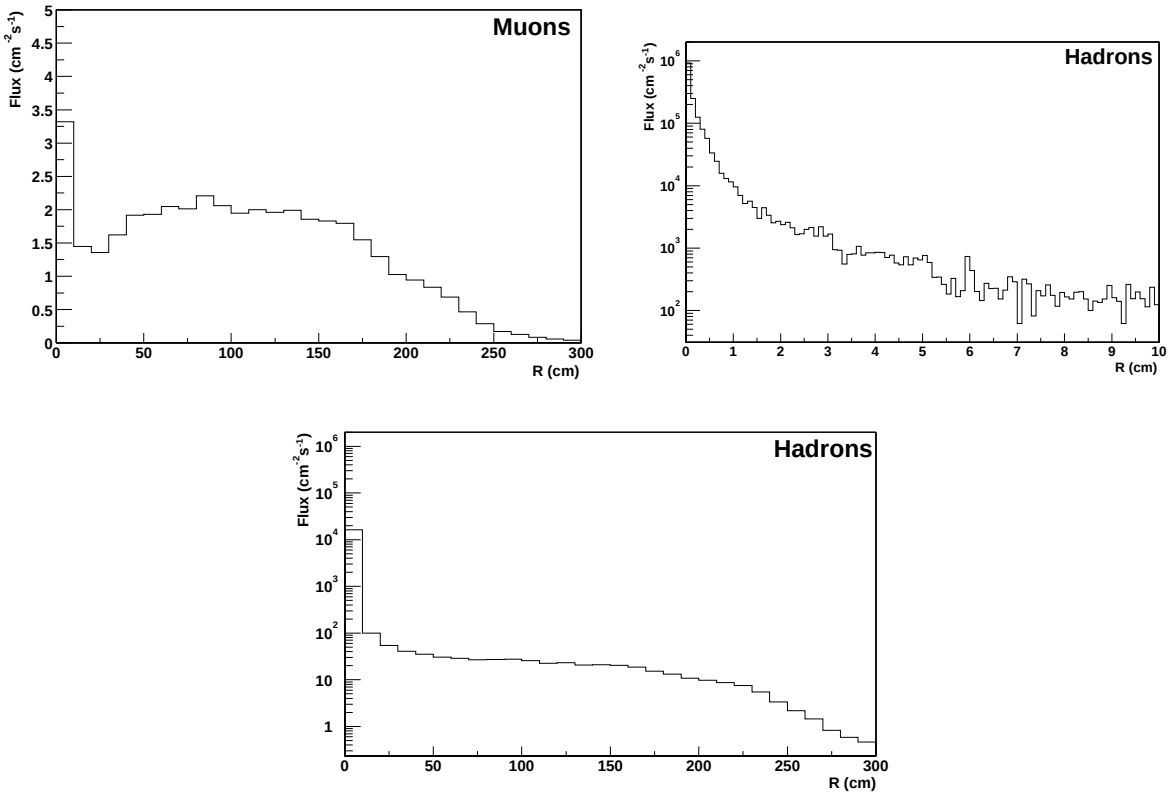

Figure 2.7: Hadron and muon flux at the tunnel entrance as a function of the distance from the beam pipe.

Table 2.5: Operation scenario for a ten-year run period, where $\langle L \rangle$ is mean luminosity, and σ_{inel} is the inelastic cross-section.

	pp	Ar–Ar	Ar–Ar	Pb–Pb	dPb
$\langle L \rangle$ (cm^{-2}s^{-1})	3×10^{30}	3×10^{27}	10^{29}	10^{27}	8×10^{28}
σ_{inel} (mb)	70	3000	3000	8000	2600
Rate (s^{-1})	2×10^{5}	9×10^{3}	3×10^{5}	8×10^{3}	2×10^{5}
Runtime (s)	10^{8}	1.0×10^{6}	2.0×10^{6}	5×10^{6}	2×10^{6}
Events	2×10^{13}	9×10^{9}	6×10^{11}	4×10^{10}	4×10^{11}
N_{ch} per event	100	2400	2400	14 200	500
N_{ch}	2.1×10^{15}	2.2×10^{13}	1.4×10^{15}	5.7×10^{14}	2×10^{14}

In order to estimate the overall radiation load on the ALICE detector, typical volumes (scoring regions) were identified, generally the location of the detector electronics: Inner Tracking System (ITS) comprising Silicon Pixel Detector (SPD), Silicon Drift Detector (SDD) and Silicon Strip Detector (SSD); the Time Projection Chamber (TPC) in the region where the electronics is situated; the Transition Radiation Detector (TRD), the Time-Of-Flight detector (TOF); the Ring Imaging CHerenkov counter (RICH) and four electronics rack locations (RackLoc1 $-$ 4). The racks are located in the following areas: RackLoc1 is on platforms situated inside the experimental area, 12 m above the floor level at the side of the L3 magnet; RackLoc2 is on the floor of the experimental area UX25 on both sides (RB24, RB26) of the L3 magnet; RackLoc3 is in four levels of counting rooms in the main access shaft PX24 and RackLoc4 is in the shielding plug PX24.

The deposited energy and the total neutron fluence, including thermal neutrons, were simulated with the FLUKA Monte-Carlo code [13] for each of the selected volumes and beams. The geometry includes the main structural elements and a detailed description of the absorbers. The DPMJET-II model [14] was used for the simulation of the pp interactions while the nucleus–nucleus collisions were generated with HIJING [15].

The results are shown in Table 2.6 with all values normalized to the ten-year scenario above. The pixel detectors close to the beam receive the highest dose, up to 200 krad (2 kGy) and 2×10^{12} neutrons/cm^2, over ten years. Since the radiation load scales approximately with $1/r^2$, doses for the other subsystems can also be estimated from this table.

2.7.3 Background from thermal neutrons

In Pb–Pb collisions at a luminosity of 10^{27} cm^{-2}s^{-1}, the primary particle production rate is 2×10^8 Hz. Many of these particles produce secondaries through hadronic and electromagnetic cascades in the absorbers and structural elements of ALICE. In particular, neutrons are copiously produced. Highly-energetic neutrons lose energy in subsequent scatterings to finally produce a gas of thermal neutrons. Each minimum bias event produces approximately 50 thermal neutrons per m^2 at a radius of 5 m in ALICE central region.

Since the average time between two subsequent Pb–Pb collision, $\simeq 100\,\mu$s, is much larger than the decay time of the neutron signal, we do not expect any substantial build-up of the thermal neutron fluency in the ALICE experimental regions. Only detectors using materials with high capture cross-sections could experience an increase of event uncorrelated background.

We have identified one such detector, the TRD, which uses Xe as a drift gas. The capture cross-section for low-energetic neutrons has resonance peaks up to 50 kb for some of the isotopes, followed by a multi-gamma de-excitation cascade. These gammas in turn can create low-energy electrons as they Compton scatter in the Xe gas, create secondary electrons or convert into electron–positron pairs. This will be a source of event uncorrelated background in the TRD.

An intensive study was performed to estimate the level of this background [16]. As a result, the number of particles per TRD layer is expected to increase by not more than 10%. Given the particular topology of the hit pattern produced by low-energetic electrons spiraling along the beam-direction, this background contribution cannot be neglected.

2.8 Luminosity determination in ALICE

The luminosity L is a quantity which relates the rate R of a process to its cross-section σ

$$R = L\sigma \quad . \tag{2.5}$$

Table 2.6: Doses and neutron fluences in detectors and electronic racks.

System	Radius (cm)	Dose (Gy)	Neutron fluence (cm^{-2})
SPD1	3.9	$(2.09 \pm 0.07) \times 10^{3}$	$(1.75 \pm 0.05) \times 10^{12}$
SPD2	7.6	$(7.91 \pm 1.21) \times 10^{2}$	$(8.71 \pm 2.61) \times 10^{11}$
SDD1	14	$(3.11 \pm 0.75) \times 10^{2}$	$(7.01 \pm 4.43) \times 10^{11}$
SDD2	24	$(1.53 \pm 0.11) \times 10^{2}$	$(6.21 \pm 2.52) \times 10^{11}$
SSD1	40	$(5.63 \pm 2.36) \times 10^{1}$	$(4.18 \pm 1.53) \times 10^{11}$
SSD2	45	$(3.56 \pm 1.98) \times 10^{1}$	$(3.48 \pm 2.17) \times 10^{11}$
TPC(el)	74	$(2.12 \pm 0.51) \times 10^{1}$	$(1.41 \pm 0.71) \times 10^{11}$
TRD	320	$(4.54 \pm 2.44) \times 10^{0}$	$(4.35 \pm 2.61) \times 10^{10}$
PID	350	$(6.36 \pm 3.21) \times 10^{0}$	$(1.71 \pm 0.91) \times 10^{10}$
HMPID	490	$(2.65 \pm 1.22) \times 10^{-1}$	$(7.30 \pm 4.78) \times 10^{9}$
RackLoc1		$(5.55 \pm 3.22) \times 10^{0}$	$(8.43 \pm 6.44) \times 10^{7}$
RackLoc2		$(3.76 \pm 3.06) \times 10^{-1}$	$(1.48 \pm 1.03) \times 10^{6}$
RackLoc3		$(2.24 \pm 1.53) \times 10^{-6}$	$(3.48 \pm 2.97) \times 10^{3}$
RackLoc4		$(7.82 \pm 5.21) \times 10^{-6}$	$(9.21 \pm 7.11) \times 10^{3}$

It is entirely defined by the characteristics of the colliding beams at the interaction point

$$L = f N_{\mathrm{b}} \frac{N^2}{2\pi(\sigma_1^2+\sigma_2^2)} F \quad , \tag{2.6}$$

where f is the revolution frequency, N_{b} the number of bunches, N the number of particles per bunch, $\sigma_{1,2}$ the transverse beam sizes of the two beams. The factor F is due to the finite crossing angle ϕ and depends on the ratio between longitudinal, σ_{l}, and transverse, σ_{t}, beam sizes

$$F = \frac{1}{\sqrt{1+\left(\frac{\tan(\phi/2)\sigma_{\mathrm{l}}}{\sigma_{\mathrm{t}}}\right)^2}} \quad . \tag{2.7}$$

Thus, measuring the beam parameters is one way of determining the luminosity. The accuracy, $\simeq 10\%$, is limited by the extrapolation of σ_{t} from measurements of beam profiles elsewhere to the interaction point.

Another way consists in measuring the rate of a well-known process. Through the optical theorem, one obtains a relation between the rate of elastic events, R_{el}, in the forward direction, i.e. momentum transfer $\sqrt{t}=0$, and the total rate of pp interactions R_{tot}:

$$L = \frac{(1+\rho^2)}{16\pi} \frac{R_{\mathrm{tot}}^2}{(\mathrm{d}R_{\mathrm{el}}/\mathrm{d}t)_{t=0}} \tag{2.8}$$

where ρ is the ratio of the real to imaginary part of the elastic-scattering forward amplitude. The measurement of the elastic rate at zero momentum transfer requires a specialized very forward experiment. It uses a dedicated beam optics with low beam divergence at the interaction point [17]. At the LHC, the TOTEM collaboration [18] will perform such a measurement. For heavy-ion collisions there exist two cross-sections that can be calculated with sufficient precision: the total hadronic cross-section and the cross-section of mutual electromagnetic dissociation. In the following sections we will discuss the luminosity determination with ALICE for pp and A–A collisions separately.

2.8.1 Luminosity monitoring in pp runs

The TOTEM experiment [18] will measure the total cross-section σ_{tot} at the LHC. In ALICE, we will measure and monitor the luminosity by measuring a fraction $R = Acc \cdot R_{\mathrm{tot}}$ of the rate of inelastic interaction. Then luminosity

$$L = \frac{R}{Acc \cdot \sigma_{\mathrm{inel}}} \tag{2.9}$$

where Acc is the detector acceptance. In reality the inelastic rate is the sum of the rates of the inelastic non-diffractive (R_{nd}), the single-diffractive (R_{sd}) and the double-diffractive (R_{dd}) processes. The detector acceptance is different for each of these processes (Fig. 2.8). Using our V0 scintillator array we can trigger on about 86% of the total inelastic hadronic cross-section, 95% of the non-diffractive and 45% of the diffractive. The Monte-Carlo simulations can be tuned to the angular track distributions measured by TOTEM. Experience from the Tevatron shows that the error on the acceptance can be reduced to a few percent and that the total uncertainty on the measured luminosity, is dominated by the error on $\delta\sigma_{\mathrm{inel}}/\sigma_{\mathrm{inel}} \simeq 5\%$.

During high-intensity proton runs, the background from beam–gas interactions could be so high that the pp trigger has to be validated by a T0 trigger. T0 is able to reject beam–gas interactions due to its capability to reject collisions outside the nominal interaction region. Having a much smaller angular acceptance than the V0 it can trigger on only 70% of the inelastic non-diffractive interactions and on 10% of the diffractive events. Low-intensity pp runs with reduced beam–gas interaction rate will be instrumental in calibrating the T0 trigger in order to achieve a similar accuracy as with the V0 trigger.

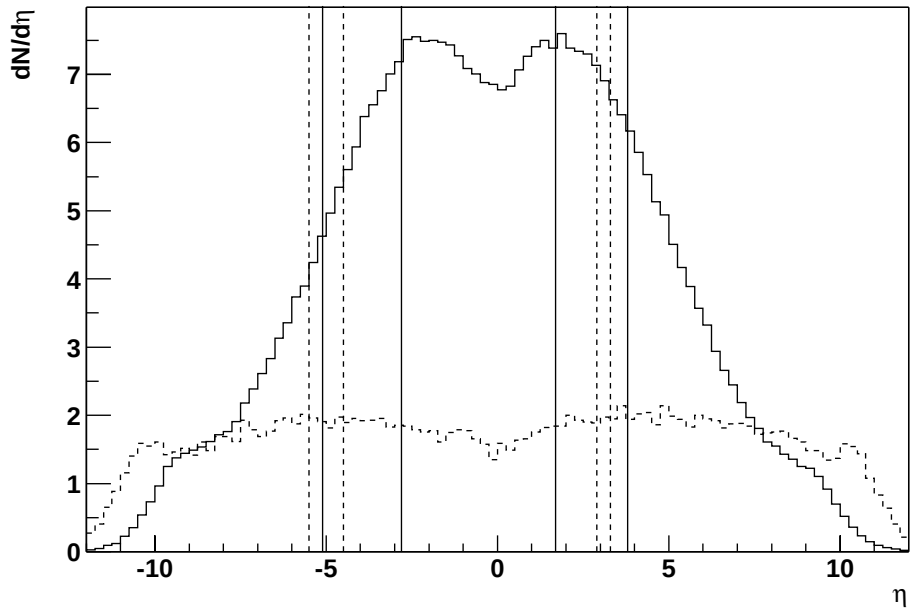

Figure 2.8: Charged-particle pseudorapidity distribution for pp interactions at $\sqrt{s} = 14\,\mathrm{TeV}$. Solid line: inelastic non-diffractive interactions, dashed line: diffractive interactions. The vertical lines indicate the acceptance of the forward detectors V0 (solid lines) and T0 (dashed lines).

2.8.2 Luminosity monitoring in Pb–Pb runs

Two interactions cross-sections known with reasonable accuracy can be used for luminosity determination in heavy-ion collisions. The total hadronic cross-section σ_{had} is mainly given by the geometry of the colliding nuclei and is known with an accuracy better than 10%. Hence, measuring the hadronic interaction rate R_{had} will allow to calculate the luminosity, $L = R_{\mathrm{had}}/\sigma_{\mathrm{had}}$. Of course, the measurement is only sensitive up to some maximum impact parameter, thus there will be an additional small systematic error from extrapolating to the total rate. The second possibility is to measure the rate of electromagnetic dissociation.

Using electromagnetic dissociation to measure and monitor the luminosity in heavy-ion colliders has been proposed in Ref. [19]. According to this method, the rate of mutual electromagnetic dissociation events $R_{\mathrm{m}}^{\mathrm{ED}}$ measured by means of Zero Degree Calorimeters (ZDC) provides the luminosity value:

$$L = \frac{R_{\mathrm{m}}^{\mathrm{ED}}}{\sigma_{\mathrm{m}}^{\mathrm{ED}}}. \tag{2.10}$$

The method relies on the accuracy with which the mutual electromagnetic dissociation cross $\sigma_{\mathrm{m}}^{\mathrm{ED}}$ is computed from theory. Simultaneous forward–backward single neutron emission from each of the collision partners provides a clear signal of the mutual dissociation process. For the most part this process proceeds through the absorption of virtual photons emitted by collision partners which is followed by the excitation and subsequent decay of the Giant Dipole Resonances (GDR) in both of the colliding nuclei. In heavy nuclei, like Au or Pb, the single neutron emission channel (1n) is the main mechanism of GDR decay. The same basic idea has been adopted for luminosity measurement and monitoring in the ALICE ZDC. We refer the reader to Ref. [20] for an extended technical description of the ALICE ZDC.

Table 2.7: Sensitivity of the mutual electromagnetic dissociation cross-sections to the equivalent photon-energy range, the probability of direct neutron emission in the 1n channel, $P_{\mathrm{n}}^{\mathrm{dir}}$, the photo-nuclear cross sections and the next-to-leading-order (NLO) corrections. The results obtained with the GNASH and RELDIS codes are given for 5.5 TeV per nucleon Pb–Pb collisions. The recommended values are those in the last column. The prediction of Ref. [19] for $\sigma_{\mathrm{m}}^{\mathrm{ED}}(1\mathrm{n} \mid 1\mathrm{n})$ is given for comparison.

	Cross-section (mb)				
	$E_\gamma \leq 24$ MeV LO	$E_\gamma \leq 140$ MeV LO		Full range of E_γ LO + NLO	
	RELDIS $P_{\mathrm{n}}^{\mathrm{dir}} = 0$	GNASH	RELDIS $P_{\mathrm{n}}^{\mathrm{dir}} = 0$	RELDIS $P_{\mathrm{n}}^{\mathrm{dir}} = 0$	RELDIS $P_{\mathrm{n}}^{\mathrm{dir}} = 0.26$
$\sigma_{\mathrm{m}}^{\mathrm{ED}}(1\mathrm{nX} \mid 1\mathrm{nY})$	519 533 [19]	488	544	727	805
$\sigma_{\mathrm{m}}^{\mathrm{ED}}(1\mathrm{nX} \mid 2\mathrm{nY})+$ $\sigma_{\mathrm{m}}^{\mathrm{ED}}(2\mathrm{nX} \mid 1\mathrm{nY})$	154	220	217	525	496
$\sigma_{\mathrm{m}}^{\mathrm{ED}}(2\mathrm{nX} \mid 2\mathrm{nY})$	11	24	22	96	77
$\sigma_{\mathrm{m}}^{\mathrm{ED}}(\mathrm{LMN})$	684	732	783	1348	1378

2.8.2.1 Cross-sections predicted by the RELDIS model

In Refs. [21,22], the RELDIS results were tested by studying their sensitivity to the variation of input data and parameters. Corrections for the next-to-leading order (NLO) processes of mutual dissociation were also taken into account. In addition to GDR excitation, quasi-deuteron absorption, Δ photo-excitation and multiple-pion photo-production were considered in different regions of equivalent photon energy, E_γ. A good description of the existing data on single dissociation of lead and gold nuclei at the CERN SPS was obtained [23, 24].

Particularly, the photo-nuclear cross-sections for specific neutron emission channels were calculated by two different models of photo-nuclear reactions, the GNASH code [25] and the RELDIS code itself, see Tab. 2.7 and Refs. [21, 22] for details. Additionally, in the latter model two different probabilities of direct neutron emission in the 1n channel, $P_{\mathrm{n}}^{\mathrm{dir}}$ were assumed.

The model also defines the cumulative value, Low Multiplicity Neutron (LMN) emission cross-section,

$$\begin{aligned}\sigma_{\mathrm{m}}^{\mathrm{ED}}(\mathrm{LMN}) = \sigma_{\mathrm{m}}^{\mathrm{ED}}(1\mathrm{nX} \mid 1\mathrm{nY}) + \sigma_{\mathrm{m}}^{\mathrm{ED}}(1\mathrm{nX} \mid 2\mathrm{nY}) + \\ \sigma_{\mathrm{m}}^{\mathrm{ED}}(2\mathrm{nX} \mid 1\mathrm{nY}) + \sigma_{\mathrm{m}}^{\mathrm{ED}}(2\mathrm{nX} \mid 2\mathrm{nY})\end{aligned} \tag{2.11}$$

where X and Y denote any other particle than a neutron. The LMN cross section was varied over several regions of equivalent photon energy in the GDR region, $E_\gamma < 24$ MeV, for the GDR and quasi-deuteron absorption region, $E_\gamma < 140$ MeV, and for the full range of E_γ.

As shown in Tab. 2.7, the ambiguity in the $1\mathrm{n} - 1\mathrm{n}$ correlated emission cross-section, $\sigma_{\mathrm{m}}^{\mathrm{ED}}(1\mathrm{nX} \mid 1\mathrm{nY})$, is up to 10% mainly due to the uncertainty in the measured photo-neutron cross-section. However, the ambiguity is reduced to $\sim 2\%$ if the sum of the one and two neutron emission channels, $\sigma_{\mathrm{m}}^{\mathrm{ED}}(\mathrm{LMN})$, is considered. As shown in Refs. [21, 22], $\sigma_{\mathrm{m}}^{\mathrm{ED}}(\mathrm{LMN})$ is also more stable with respect to other input parameters compared to $\sigma_{\mathrm{m}}^{\mathrm{ED}}(1\mathrm{nX} \mid 1\mathrm{nY})$ and other cross-sections. Therefore, $\sigma_{\mathrm{m}}^{\mathrm{ED}}(\mathrm{LMN})$ represents a cumulative neutron emission rate which should be used for the luminosity measurement at heavy-ion colliders.

References

[1] D. Brandt, LHC Project Report 450.
[2] H. Meier et al., Phys. Rev. **A63** (2001).
[3] A. Morsch, Internal Note, ALICE-INT-2002-32.
[4] B. Jeanneret, Beam Physics Note 41.
[5] P. Giubellino et al., Internal Note, ALICE-INT-2000-28.
[6] J.-P. Revol, EPJdirect C, **4**(S1) (2002) 14.
[7] I. Baichev, private communications.
[8] A. Morsch, Internal Note, ALICE-INT-97-13.
[9] A. Rossi, private communications.
[10] L.R. Collins and O.B. Malyshev, LHC Project Note 274.
[11] I. Azhgirey et al., LHC Project Note 273.
[12] B. Pastircak, Alice Internal Note, ALICE-INT-2002-xx.
[13] A. Fassó, A. Ferrari, J. Ranft, P. Sala, *New developments in* FLUKA *modelling of hadronic and EM interactions. In Proceedings of the third workshop on simulating accelerator radiation environments(SARE-3)*, KEK, Tsukuba, Japan, 1997, p.32 (1997).
[14] J. Ranft, Phys. Rev. **D51** (1995) 64.
J. Ranft, *DPMJET-II, a Dual Parton Model event generator for hadron-hadron, hadron-nucleus and nucleus-nucleus collisions*, Presented at SARE2 Workshop, CERN, 9-11 October, 1995, Proceedings: CERN/TIS-RP/97-05 (1997).
[15] X. N. Wang and M. Gyulassy, Phys. Rev. **D44** (1991) 3501.
M. Gyulassy and X. N. Wang, Comput. Phys. Commun. **83** (1994) 307-331.
[16] G. Tsiledakis, Y. Foka, A. Morsch, A. Sandoval, Alice Internal Note, ALICE-INT-2002-xx.
[17] A. Fauss-Golfe et al., Proceedings of EPAC 2002, Paris, France (2002) 320.
[18] W. Kienzle et al. - TOTEM Collaboration, *TOTEM, Total Cross Section, Elastic Scattering and Diffraction Dissociation at the LHC*,
Technical Proposal, CERN-LHCC-99-007, LHCC-P-5.
[19] A.J. Baltz, C. Chasman, S.N. White, Nucl. Instr. Meth. **A417** (1998) 1.
[20] ALICE Collaboration, *Technical Design Report of the Zero Degree Calorimeter (ZDC)*, CERN/LHCC 99-5, ALICE TDR3, March 1999
[21] I.A. Pshenichnov, J.P. Bondorf, I.N. Mishustin, A. Ventura, S. Masetti, Phys. Rev. **C64** (2001) 024903.
[22] I.A. Pshenichnov, J.P. Bondorf, A.B. Kurepin, I.N. Mishustin, A. Ventura, ALICE Internal Note, ALICE-INT-2002-07.
[23] H. Dekhissi, G. Giacomelli, M. Giorgini, S. Manzoor, L. Patrizii, V. Popa, P. Serra, V. Togo, Nucl. Phys. **A662** (2000) 207.
[24] J.C. Hill, A. Petridis, B. Fadem, F.K. Wohn, Nucl. Phys. **A661** (1999) 313c.
[25] P.G. Young, E.D. Arthur, M.B. Chadwick: in *Nuclear Reaction Data and Nuclear Reactors*, edited by A. Gandini and G. Reffo, World Scientific, Singapore, 1998, Vol. I, p. 227